Water oxidation utilizing a ruthenium complex featuring a phenolic moiety inspired by the oxygen-evolving centre (OEC) of photosystem II

Supporting Information

Yugo Kumagai[a], Risa Takabe[a], Takashi Nakazono[b], Mitsuo Shoji*[c], Hiroshi Isobe[d], Kizashi Yamaguchi[e,f], Tomoyo Misawa-Suzuki[g], Hirotaka Nagao[g], and Tohru Wada*[a]

[a]Department of Chemistry, College of Science, Rikkyo University, 3-34-1, Nishi-Ikebukuro, Toshima-ku, Tokyo, 171-8501, Japan. E-mail: twada@rikkyo.ac.jp

[b]Research Center for Artificial Photosynthesis (ReCAP), Osaka Metropolitan University, 3-3-138 Sugimoto, Sumiyoshi-ku, Osaka 558-8585, Japan. E-mail: nakazono@omu.ac. Jp

[c]Center for computational Sciences, University of Tsukuba, Tennodai 1-1-1, Tsukuba 305-8577, Japan. E-mail: mshoji@ccs.tsukuba.ac.jp

[d]Research Institute for Interdisciplinary Science, Okayama University, Okayama 700-8530, Okayama, Japan

[e]SANKEN, Osaka University, Ibaraki 567-0047, Osaka, Japan

[f]Center for Quantum Information and Quantum Biology (QIQB), Osaka University, Toyonaka 560-0043, Osaka, Japan

[g]Department of Materials and Life Sciences, Faculty of Science and Technology, Sophia University, 7-1, Kioi-cho, Chiyoda-ku, Tokyo, 102-8554, Japan. E-mail: h-nagao@sophia.ac.jp

Contents:

S1 Experimental Section

Anthraquinone-1,8-dibronic acid[1] and 4'-(trifluoromethylsulfonyl)oxy}-2,2':6',2"-terpyridine[2] were prepared according to literatures. [Ru(OH$_2$)(bpy)(trpy)](BPh$^F_4$)$_2$ was synthesized through the anion exchange reaction of [Ru(OH$_2$)(bpy)(trpy)](ClO$_4$)$_2$ prepared according to the literature[3] with NaB BPh$^F_4$ (Sigma-Aldrich Inc.). All compounds were synthesized using commercial-grade reagents and solvents without any further purification. All other reagents and solvents were purchased from Kanto Chemical Co. Inc. Elemental analyses were performed using a Vario Micro Cube (Elementar Analysensysteme GmbH). ESI-TOF-MS spectra were recorded on a JEOL JMS-T100LP AccuTOF (JEOL Ltd.).

Synthesis of [1](PF$_6$)$_2$

A synthetic scheme of [1](PF$_6$)$_6$ was depicted to Scheme S1
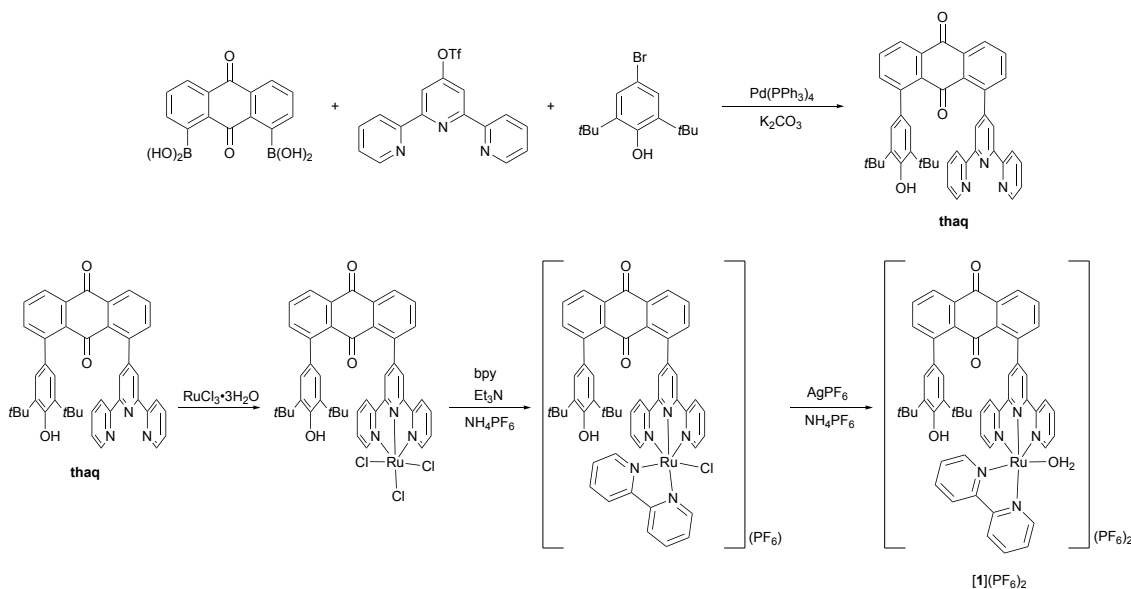
Scheme S1. Synthetic scheme of [1](PF$_6$)$_2$

1-(2,2':6',2"-terpyrid-4'-yl)-8-(2,6-*tert*-butyl-*p*-hyrodoxyphenyl)anthraquinone (thaq). N$_2$ bubbling procedure was carried out on a solution comprising 30 mL of toluene, ethanol, and 4.8 mL of distilled water containing 1,8-anthracene diboronic acid (100 mg, 0.34 mmol), 4-bromo-2,6-di-*tert*-butylphenol (96 mg, 0.34 mmol), 4'-{(trifluoromethylsulfonyl)oxy}-2,2':6',2"-terpyridine (129 mg, 0.34 mg), and potassium carbonate (331 mg, 2.39 mmol) within a Schlenk flask for 30 minutes to eliminate O$_2$ from the solution. Subsequently, Pd(PPh$_3$)$_4$ (39 mg, 0.033 mmol, 5 mol% for a boronic acid of 1,8-anthracene diboronic acid) was introduced into the reaction mixture, and the solution was refluxed under a nitrogen atmosphere for 24 hours. The resulting solution underwent evaporation to dryness. The residue was added to 10 mL of water, and the pH was adjusted using aqueous HCl.

Extraction with $CHCl_3$ followed, and the solution was subjected to filtration using a phase-separating filter. The organic phase was then evaporated to dryness. The residue underwent purification through silica-gel column chromatography (Silica-gel 60N, Kanto Chemical Co., Inc.), utilizing $CHCl_3$ as the eluent. The yield obtained was 110 mg, representing a 50% yield. Anal. Calc. for $C_{43}H_{37}N_3O_3 \cdot 1/2CH_3OH$ (659.81): C 79.19, H 5.96, N 6.37; found: C 79.44, H 5.67, N 6.49. ^{1}H NMR (400 MHz, in $CDCl_3$): δ(ppm), 1.14 (s, 18H, tBu), 5.01 (s, 1H, OH), 6.90 (s, 2H, phenol), 7.32 (ddd, 2H, J^1 = 7.6, J^2 = 5.6, J^3 = 1.2, trpy), 7.56 (ddd, 2H, J^1 = J^2 = 7.6 Hz, J^2 = 1.2 Hz, trpy), 7.69 (dd, 1H, J^1 = J^2 = 8.0 Hz, anthraquinone), 7.76 (dd 1H, J^1 = J^2 = 8.0 Hz, anthraquinone), 7.87 (ddd, 2H, J^1 = 7.6, J^2 = 1.6Hz, trpy), 8.34 (dd, 1H, J^1 = 8.0, J^2 = 1.2 Hz, anthraquinone), 8.36 (s, 2H, trpy), 8.43 (dd, 1H, J^1 = 8.0, J^2 = 1.6 Hz, anthraquinone), 8.63 (d, 2H, J = 5.6 Hz, trpy), 8.67 (d, 2H, J = 8.0 Hz, anthraquinone). DART-MS: m/z = 644.4 ([M] + H$^+$, Calc. 644.3). We depicted the ^{1}H-NMR spectrum of thaq in Figure S1.

RuCl₃(thaq). A 15 mL ethanol solution containing $RuCl_3 \cdot 3H_2O$ (24 mg, 90 μmol) underwent reflux for a duration of 5 minutes under a nitrogen atmosphere. Subsequently, thaq (51 mg, 79 μmol) was introduced to the solution, which had been cooled to room temperature. The resulting mixture was subjected to reflux for a period of 30 minutes under a nitrogen atmosphere. A precipitate brown powder was isolated by filtration, followed by washing with ethanol, water, and diethyl ether. The obtained yield was 61 mg, corresponding to an 89% yield. Anal. Calc. for $C_{35}H_{19}Cl_3N_3O_3Ru \cdot 3C_2H_5OH$ (874.08): C 56.27, H 4.26, N 4.80; found: C 56.27, H 4.32, N 4.60.

[RuCl(bpy)(thaq)](PF₆). N_2 bubbling was applied to a suspension comprising [RuCl₃(thaq)] (28 mg, 32 μmol), 2,2'-bipyridine (5.4 mg, 3.5 μmol), and LiCl (14 mg, 330 μmol) in a mixture of ethanol and distilled water (22 mL/8 mL) for a duration of 15 minutes to eliminate O_2. Following the addition of Et₃N (9.2 μL, 66 μmol) to the suspension, a subsequent influx of N_2 gas was sustained for an additional 30 minutes. The resulting suspension underwent reflux for a period of 16 h. Upon filtration of the heated reaction mixture, a saturated aqueous solution of NH_4PF_6 was introduced to the filtrate. Evaporation of the solution under reduced pressure led to the precipitation of a dark reddish-brown solid, subsequently subjected to purification through column chromatography employing acidic alumina (MP Alumina A, Act. I acid pH, MP Biomedicals inc.) and acetone as eluents. The yield obtained was 23 mg, representing a 69% yield. Anal. Calc. for $C_{53}H_{45}ClF_6N_5O_3PRu \cdot 2CH_3OH$ (1145.54): C 57.67, H 4.66, N 6.11; found: C 57.42, H 4.52, N 5.97. ^{1}H NMR (400 MHz, in Acetone-d₆): δ(ppm), 1.14 (s, 18H, tBu), 5.95 (s, 1H, OH), 6.74 (dd, 1H, J = J = 6.4 Hz, anthraquinone), 7.17 (s, 2H, phenol), 7.23 (d, 1H, J = 5.2 Hz, anthraquinone), 7.40 (ddd, 2H, J^1 = J^2 = 6.4, J^3 = 0.8 Hz, trpy), 7.67 (dd, 1H, J^1 = 6.4Hz, J^2 = 1.2Hz, bpy), 7.79 (ddd, 1H, J^1 = J^2 =8.0, J^3 = 1.2Hz, bpy), 7.84 (d, 2H, J = 5.6 Hz, trpy), 7.90 (dd, 1H, J^1 = J^2 = 8.0Hz, bpy), 8.00 (m, 2H, bpy), 8.08 (m, 1H, trpy), 8.12 (t, J = 8.0 Hz, 1H, bpy), 8.36 (m, 1H, anthraquinone), 8.43 (m, 1H, bpy), 8.43 (m, 1H, anthraquinone), 8.57 (d, 2H, J = 0.8 Hz, trpy),

8.60 (t, J = 8.0 Hz, 1H, anthraquinone), 8.73 (s, 2H, trpy), 8.86 (d, 1H, J = 8.0Hz, anthraquinone), 10.35 (d, 1H, J = 5.6Hz, bpy), ESI-MS: m/z = 936.2 ([M]$^+$, Calc. 936.2). UV-vis (in MeOH/H$_2$O = 1/1): 515 nm (ε = 1.12 x 10^4 M^{-1} cm^{-1}). We depicted the ^{1}H-NMR and UV-vis spectra of [RuCl(bpy)(thaq)](PF$_6$) in Figures S2 and S4.

[Ru(OH$_2$)(bpy)(thaq)](PF$_6$)$_2$ ([1](PF$_6$)). N$_2$ bubbling was applied to a solution comprising [RuCl(bpy)(thaq)](PF$_6$) (41 mg, 38 μmol) and AgPF$_6$ (93 mg, μmol) in a solvent mixture of acetone and distilled water (37 mL/12 mL) for a duration of 15 minutes to remove O$_2$. The ensuing solution underwent reflux for 8 h under a nitrogen atmosphere, conducted in the absence of light, to induce the precipitation of a colorless solid. The resultant suspension was subjected to filtration using celite (Celite®503, Kanto Chemical Co., Inc.). An aqueous solution of NH$_4$PF$_6$ was introduced to the filtrate and allowed to cool in a refrigerator for a day. The resultant dark reddish-brown crystals were collected via filtration and subsequently desiccated under vacuum. The yield achieved was 15 mg, corresponding to a 32% yield. Anal. Calc. for C$_{53}$H$_{47}$F$_{12}$N$_5$O$_4$P$_2$Ru·3CH$_3$OH (1305.27): C51.54, H4.56, N5.37; found: C51.42, H 4.52, N 5.26. ^{1}H NMR (400 MHz, in Acetone-d$_6$): δ(ppm), 1.05 (s, 18H, tBu), 6.66 (dd, 1H, J^1 = J^2 = 6.4 Hz, anthraquinone), 7.01 (s, 2H, phenol), 7.17 (d, 1H, J = 5.2 Hz, bpy), 7.42 (ddd, 2H, J^1 = 6.6, J^2 = 5.2 , J^3 = 1.6 Hz, J^3 = 1.6 Hz, bpy), 7.59 (dd, 1H, J^1 = 7.8 Hz, J^2 = 1.2 Hz, bpy), 7.75 (ddd, 1H, J^1 = J^2 = 7.8 Hz, J^3 = 1.6 Hz, bpy), 7.85 (d,1H, J = 7.6, Anthraquinone), 7.86 (d, J = 7.6 Hz, Anthraquinoen), 7.87 (d, 1H, J = 7.6 Hz, anthraquinone), 7.90 (dd, 1H, J^1 = 7.8, J^2 = 1.2 Hz, bpy), 8.01 (ddd, 2H, J^1 = J^2 = 7.6 Hz, J^3 = 2.0 Hz, trpy), 8.07 (dd, 1H, J = J =7.6 Hz, anthraquinone), 8.10 (ddd, 1H, J^1 = 6.6, J^2 = 5.2, J^3 = 1.2 Hz, bpy), 8.32 (dd, 1H, J^1 = 7.6, J^2 = 1.2 Hz, trpy), 8.39 (ddd, 1H, J^1 = J^2 = 7.8, J^3 = 1.6 Hz, bpy), 8.48 (dd, 2H, J^1 = 7.6, J^2 =1.2 Hz, trpy), 8.52 (dd, 2H, J^1 = J^2 = 7.6 Hz, trpy), 8.69 (s, 2H, trpy), 8.81(d, 1H, J = 7.6 Hz, anthraquinoene), 9.62 (d, 1H, J = 5.2 Hz, bpy). The 1H-NMR signal of phenolic OH was missing because of H/D exchange in aceton-d$_6$/D$_2$O solution.   ESI-MS: m/z = 450.6 ([M-(H$_2$O)]$^{2+}$, Calc. 450.6), 458.6 ([M-2H]$^{2+}$, Calc. 458.6), 459.6 ([M]$^{2+}$, Calc. 459.6), 1064.3 ([M](PF$_6$)$^+$, Calc. 1064.3). UV-vis (in MeOH/H$_2$O = 1/1): 483 nm (ε = 1.03 x 10^4 M^{-1} cm^{-1}). We depicted the ^{1}H-NMR and UV-vis spectra of [**1**](PF$_6$)$_2$ in Figures S3 and S5.

S2 Characterizations

NMR spectroscopy.

^{1}H NMR spectra were recorded on an ECX-400 spectrometer (JEOL Ltd.).

Figure S1. ^{1}H NMR (CDCl$_3$) of thaq

Figure S2. ^{1}H NMR (acetone-d$_6$) of [RuCl(bpy)(thaq)](PF$_6$)
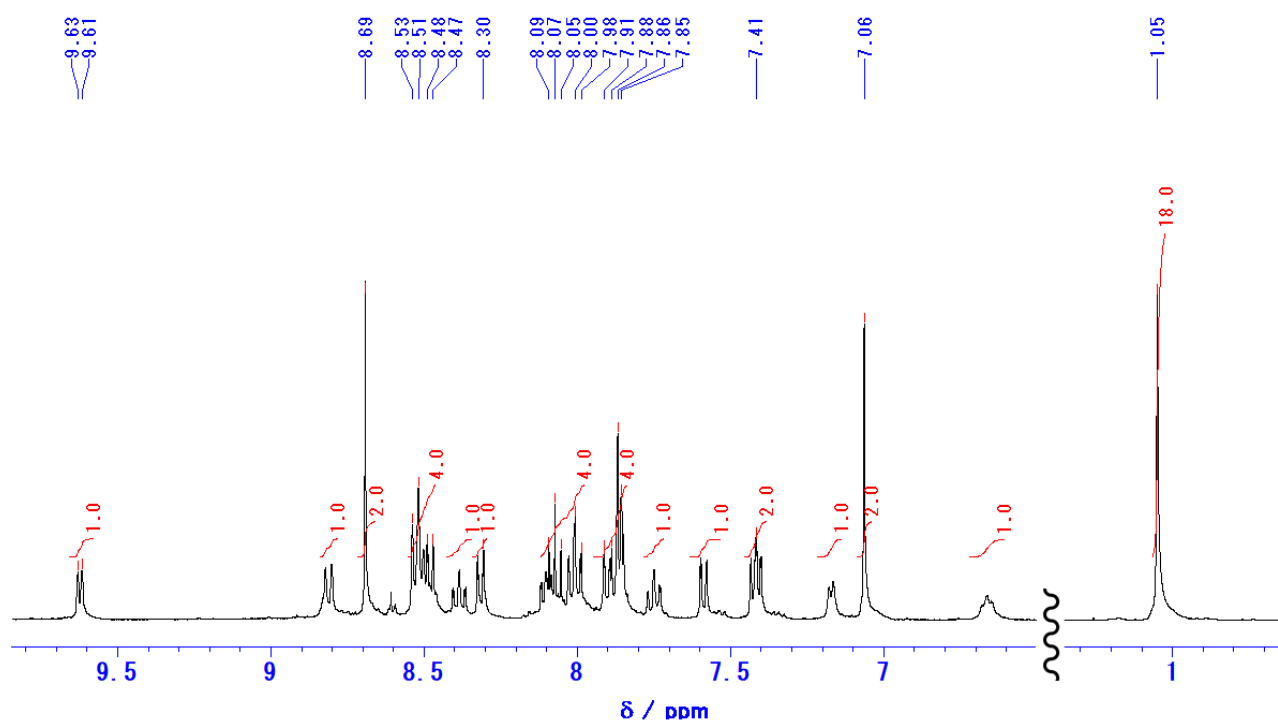
Figure S3. ^{1}H NMR (acetone-d$_6$/D$_2$O = 10/1) of [**1**](PF$_6$)$_2$

UV-Vis Spectroscopy.

UV-Vis spectra were recorded on a UV-1800 UV-VIS-NIR scanning spectrophotometer (Shimadzu Co.) using a quartz glass cell (optical pass length:10 mm) at room temperature.
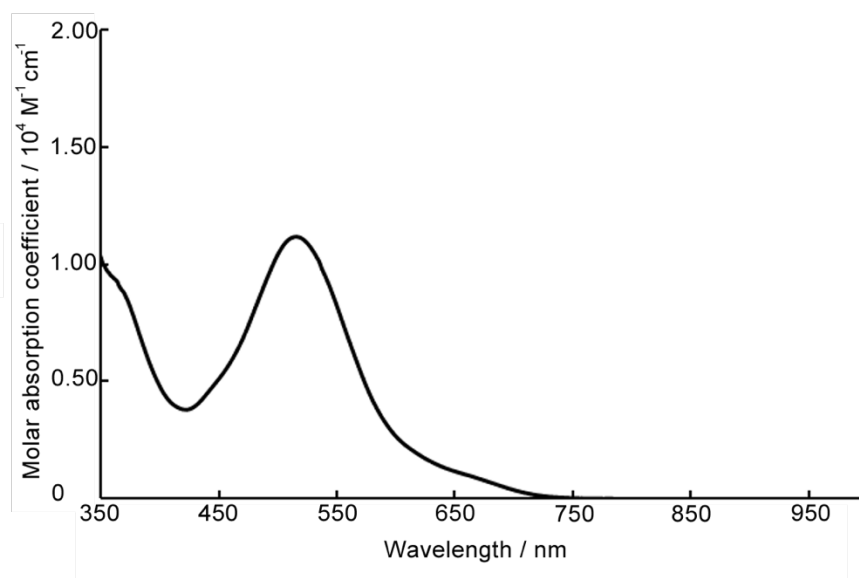
Figure S4. UV-vis spectrum of [RuCl(bpy)(thaq)](PF$_6$) in acetone

6
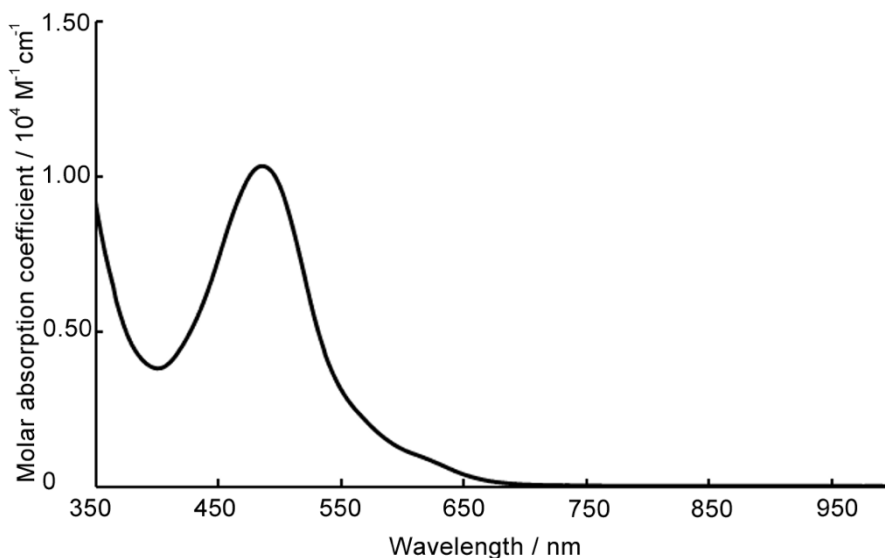
Figure S5. UV-vis spectrum of [**1**](PF$_6$)$_2$ in H$_2$O/MeOH (1/1)

Single Crystal X-ray Crystallography

Single crystals of [**1**](PF$_6$)$_2$ · 3(CH$_3$)$_2$CO · 2H$_2$O suitable for X-ray crystallography were obtained through recrystallization from a H$_2$O/acetone solution containing a large excess amount of NH$_4$PF$_6$ at room temperature. The data collection for the single crystal was conducted at 100 K utilizing a D8 QUEST diffractometer (Bruker Co.) with Mo-Kα radiation (λ = 0.71073 nm). Using Olex2[4], the structure was solved with the SHELXT[5] structure solution program using Intrinsic Phasing and refined with the SHELXL[6] refinement package using Least Squares minimization. All nonhydrogen atoms excluding a PF$_6$ counter anion and an acetone molecule underwent refinement with anisotropic atomic displacement parameters. Isotropic atomic displacement parameters were applied to one of the two PF$_6$ counter anions and one of the three acetone molecules due to considerable disorder. The crystal of [**1**](PF$_6$)$_2$·3(CH$_3$)$_2$CO·2H$_2$O exhibited Alert B in the checkcif. There is no particular trend in the hkl index for these reflections, therefore, they do not suggest a major error in the analysis. I think that these reflections were measured with inaccurate diffraction intensities due to a measurement problem. The *R*-factor remains favorable (0.0449), and the structural insights into the cationic component are entirely reliable and pertinent. The supplementary crystallographic data for CCDC2312432 ([**1**](PF$_6$)$_2$·3(CH$_3$)$_2$CO·2H$_2$O) are generously provided by The Cambridge Crystallographic Data Center at no cost. Crystal data and the structural refinement details for [**1**](PF$_6$)$_2$·3(CH$_3$)$_2$CO·2H$_2$O, along with selected bond lengths and angles, are presented in Tables S1 and S2, respectively.

7

Table S1. Crystal data and structural refinement of [**1**]$(PF_6)_2 \cdot 3(CH_3)_2 CO \cdot 2H_2O$

Empirical formula	$C_{62}H_{69}F_{12}N_5O_9P_2Ru$
Formula weight	1419.23
Temperature/K	100
Crystal system	triclinic
Space group	P-1
a, b, c /Å	12.5815(10), 13.8354(10), 20.7793(16)
α, β, γ / Å	91.668(3), 105.756(3), 111.363(2)
Volume/Å^3	3208.7(4)
Z	2
ρ_{calc} g /cm^3	1.469
μ / mm^{-1}	0.388
$F(000)$	1460.0
Crystal size/mm^3	0.7 × 0.12 × 0.09
Radiation	Mo $K\alpha$ (λ = 0.71073)
2Θ range for data collection/°	3.604 to 55.12
Index ranges	-16 ≤ h ≤ 16, -18 ≤ k ≤ 17, -27 ≤ l ≤ 27
Reflections collected	233954
Independent reflections	14759 [R_{int} = 0.1103, R_{sigma} = 0.0381]
Data/restraints/parameters	14759/60/947
Goodness-of-fit on F^2	1.079
Final R indexes [I>=2σ (I)]	$R_1{}^a$ = 0.0449, w$R_2{}^b$ = 0.0996
Final R indexes [all data]	$R_1{}^a$ = 0.00560, w$R_2{}^b$ = 0.1054
Largest diff. peak/hole / e Å^{-3}	0.81/-0.89

[a]$R = \{\Sigma(|F_o|^2 - |F_c|^2)^2/\Sigma|F_o|^2\}^{1/2}$. [b]$wR = \{\Sigma w(|F_o|^2 - |F_c|^2)^2/\Sigma w|F_o|^2\}^{1/2}$; $w = 1/\sigma^2(F_o)^2$. [c]$R_1 = \Sigma[|F_o| - |F_c|]/\Sigma$.

Table S2. Selected bond lengths and angles of [**1**](PF$_6$)$_2$·3(CH$_3$)$_2$CO·2H$_2$O

bond	Length / Å
Ru1 O1 (aqua ligand)	2.1253(17)
Ru1 N1 (terpyridine)	2.069(2)
Ru1 N2 (terpyridine)	1.965(2)
Ru1 N3 (terpyridine)	2.065(2)
Ru1 N4 (bipyridine)	2.023(2)
Ru1 N5 (bipyridine)	2.065(2)
O2 C16 (phenol)	1.371(3)
O3 C35 (anthraquinone)	1.223(3)
O4 C42 (anthraquinone)	1.215(3)
	Agnel / °
N2 Ru1 O1	89.72(8)
N2 Ru1 N3	79.28(8)
N3 Ru1 O1	87.66(7)
N5 Ru1 O1	92.70(8)

S3 Electrochemical Experiments

Cyclic and differential pulse voltammetry. Cyclic and differential pulse voltammograms were recorded on an electrochemical analyzer model 720D (ALS Co., Ltd). We performed CV and DPV experiments using a fluorine-doped tin oxide FTO coated glass electrode (purchased from Peccell Technologies, Inc.)that had been modified with the complex as a working electrode. The complex-modified working electrode was prepared by casting a acetone solution of [**1**](PF_6)$_2$ (0.10 nmol/cm^2) using a micro syringe on the FTO (0.48 cm^2), which was dried up at room temperature. Pt wire as a counter electrode, and saturated calomel electrode (SCE) as a reference electrode, in a borate buffer solution (0.05 M) (Figure 3 and 4). CVs and DPVs were carried out using a plate material evaluating cell (ALS co. Ltd) composed of the complex modified FTO, Pt wire, saturated calomel electrode (SCE) as working, counter, and reference electrodes, respectively, in the air at room temperature.
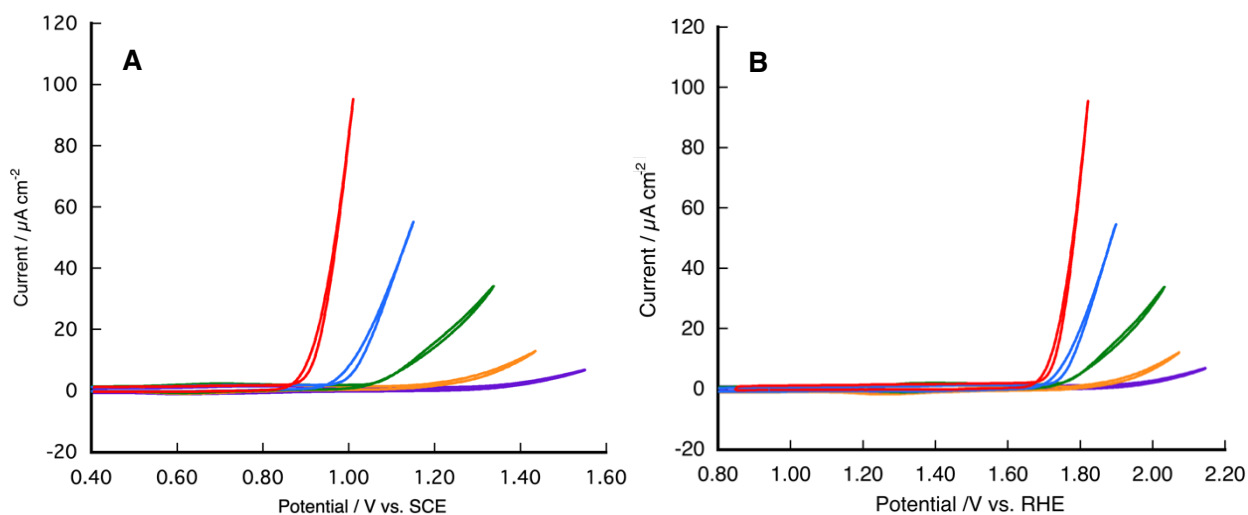
Figure S6. CVs using the FTO glass plate modified with [**1**](PF_6)$_2$ as working electrodes in boronic acid buffer solution (100 mM) at pH 10.0 (red), 9.0 (blue), 8.0 (green), 7.0 (yellow), and 6.0 (purple). Counter electrode: Pt; scan rate: 50 mV s^{-1}. temperature: 293 K. **A**: CVs referencing SCE. **B**: CVs referencing the reversible hydrogen electrode (RHE). All potentials are transformed according to the equation.: $E_{RHE} = E_{SCE} + 0.241 + 0.059 \times pH$

10

Controlled-potential electrolysis. Controlled-potential electrolysis was carried out using a compartment airtight sealing electrolysis cell (EC Frontier co., Ltd.) separated with anion exchange membrane Selemion (purchased from AGC Engineering Co., Ltd.) composing a complex modified FTO electrode (1.0×10^{-9} mol cm^{-2}, 2.25 cm^2) prepared by the cast method mentioned above, a Pt plate counter electrode (5.0 cm^2), and a SCE reference electrode. An Ar bubbling procedure was carried out on both cells comprising 30 mL of borate buffer solutions (20 mL, pH 9.0) for 30 min. All electrolysis experiments were conducted employing the airtight sealing cell within a glove bag purged with argon. The controlled-potential electrolysis of water was conducted at 1.05 V (vs. SCE) under Ar atmosphere at room temperature using EC stat 301 (EC Frontier co. Ltd.). The amount of evolved oxygen gas was determined using a FireSting Oxygen monitor (PyroScience GmbH).
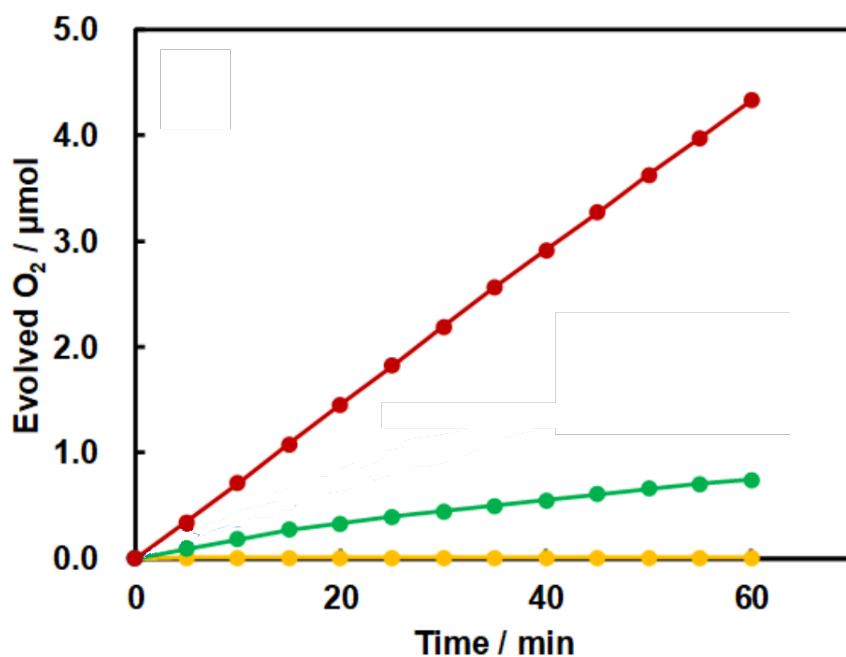
Figure S7. Current-time plots of controlled-potential electrolysis experiments using a ITO coated glass plate modified with [**1**](PF$_6$)$_2$ (red) or [**2**](BPh$^F_4$)$_2$ (green), and bare FTO coated glass plate (yellow, blank test) as a working electrode

Stability of [1](PF$_6$)$_2$ under electrolysis conditions

Raman Spectroscopy. Raman spectra were also recorded on an NRS-5100 (JASCO Co.Ltd.) with a laser (λ = 532 nm, 100 mW). Raman spectra of [1](PF$_6$)$_2$ modified on the FTO working electrode were measured before and after electrolysis for 30 min under the conditions mentioned above. These Raman spectra are completely consistent each other, indicating [1](PF$_6$)$_2$ was not decomposed during the electrolysis.
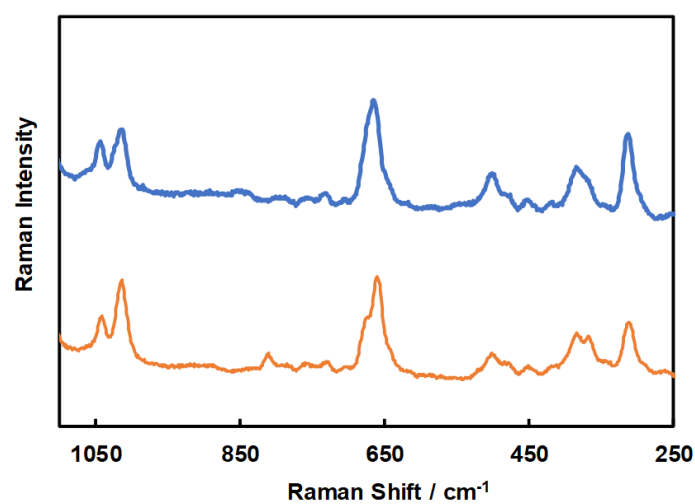
Figure S8. Raman spectra of [1](PF$_6$)$_2$ modified on the FTO working electrode before (blue) and after electrolysis for 30 min under the conditions mentioned above (orange)

S4 Chemical Oxidation of [1](PF₆)₂

Preparation of MG. Tris(2,4-dibromophenyl)aminium hexafluoroantimonate, also known as Magic Green (MG), was synthesized following the previously reported procedure.[7] MG dissolved in dichloromethane (CH₂Cl₂) exhibits a robust absorption band at 880 nm, with a molar absorptivity (ε) of 4.07. The concentration of MG in the CH₂Cl₂ solution, employed for the chemical oxidation of $[1]^{2+}$, was verified through UV-Vis spectroscopic measurements (Figure S9).
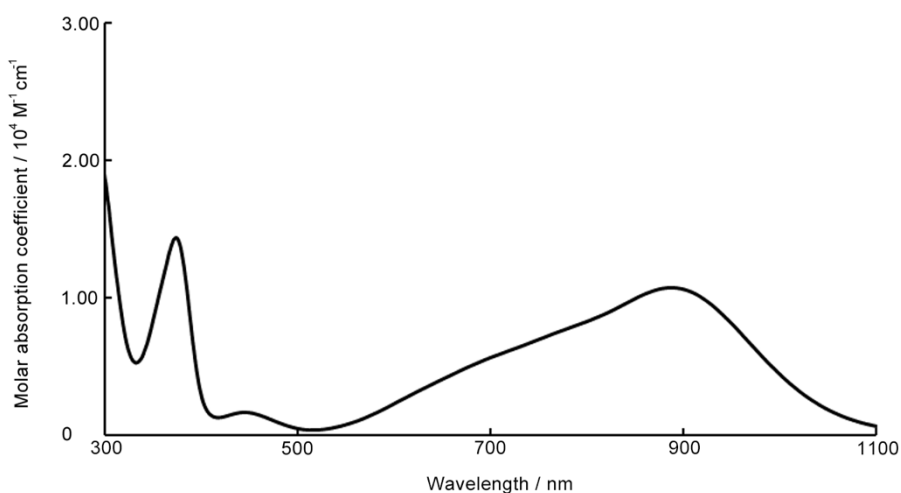
Figure S9. UV-Vis spectrum of CH₂Cl₂ solution of MG at room temperature

Chemical oxidation of [1](PF₆)₂ with MG. CH₂Cl₂ solutions (25 mM) of Magic Green (MG) were incrementally introduced into a 1.5 mL CH₂Cl₂ solution of $[1]^{2+}$ (0.10 mM) via a micro syringe at ambient temperature. UV-Vis spectra of the solutions were acquired using a UV-1800 UV-Vis-NIR scanning spectrophotometer (Shimadzu Co.) with a quartz glass cell (optical path length: 10 mm) at room temperature (Figure 6). After the addition of 3.0 equivalents of MG, a CH₂Cl₂ solution of 3,5-di-*tert*-butylcatechol (15 mM, 1.5 equiv. for $[1]^{2+}$) was introduced into the solution (Figure S10), and then ethanolic solution of HClO₄ (3 mM, 24 equiv. for for $[1]^{2+}$) was added to the solution (Figure S11).
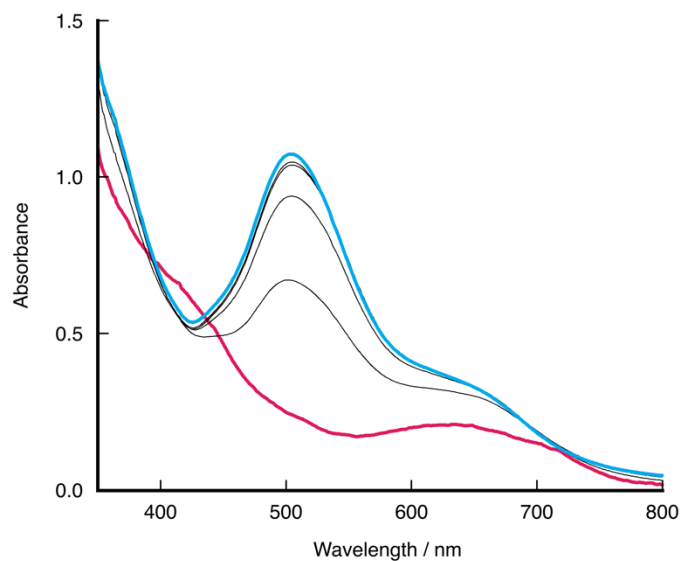
Figure S10. UV-Vis spectra of [**1**](PF$_6$)$_2$ and 3.0 equiv. of MG in CH$_2$Cl$_2$ before (red), after adding 3,5-di-*tert*-catechol (sky blue)
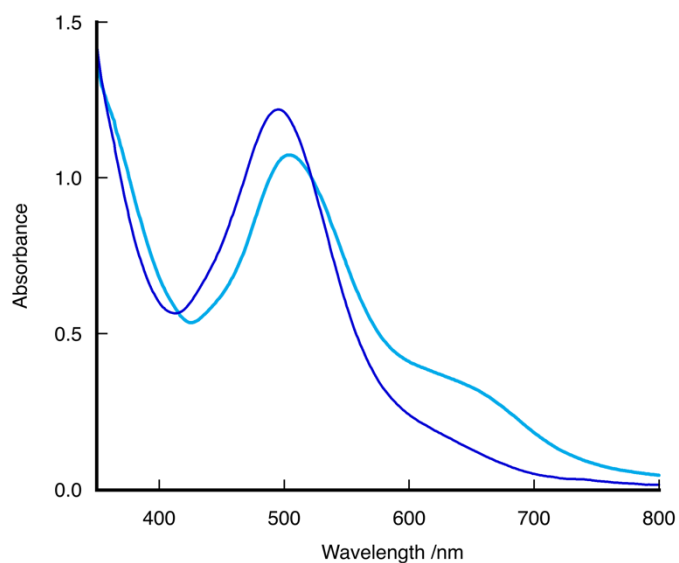
Figure S11. UV-Vis spectra of [**1**](PF$_6$)$_2$, 3.0 equiv. of MG in CH$_2$Cl$_2$, and 1.5 equiv. of 3,5-di-*tert*-catechol (sky blue). After that, HClO$_4$ was added to the solution (blue)

14

Electron Paramagnetic Resonance (EPR) Spectroscopy. CH_2Cl_2 solution of MG at a concentration of 3.0 equivalents was introduced into the CH_2Cl_2 solution of [**1**]$(PF_6)_2$ (1.0 mM) under a nitrogen atmosphere at room temperature. Subsequently, a CH_2Cl_2 solution of 3,5-di-*tert*-butylcatechol (3.0 equivalents for [**1**]$^{2+}$) was added to the solution. X-band electron EPR spectra of the frozen solution before and after the addition of MG and 3,5-di-*tert*-butylcatechol were recorded using a JES-FA300 instrument (JEOL Co. Ltd.) at 77 K (liquid nitrogen) under nonsaturating microwave power conditions. The modulation amplitude was selected to optimize the resolution and signal-to-noise ratio of the observed spectra. The g values were calibrated using a Mn^{II} marker as a reference. EPR spectra of the CH_2Cl_2 frozen solution of MG were obtained under the same experimental conditions (Figure S12).
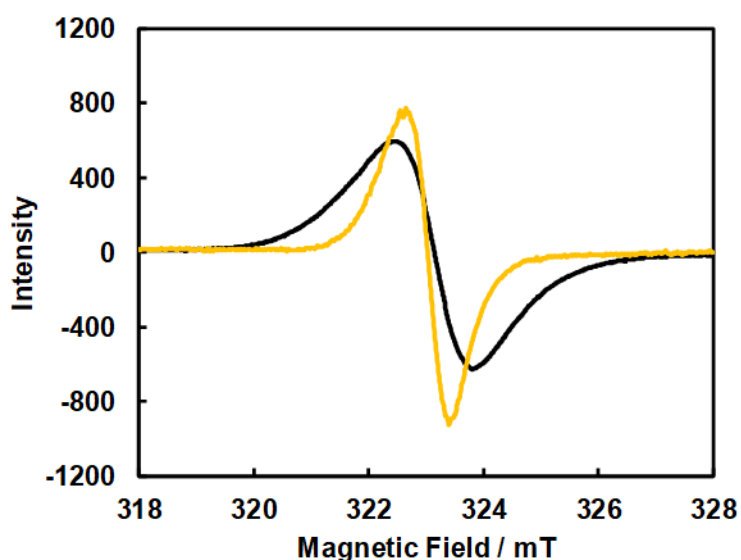
Figure S12. X-band EPR spectra of the oxidized form of [**1**]$(PF_6)_2$ (1.0 mM) with MG (yellow, this is the same as Figure 7.) and MG (black) in glassy CH_2Cl_2 at 77 K (liquid N_2). Microwave frequency, 9.029006 GHz; Microwave power, 0.9980 mW; Modulation width, 100 mT; Modulation amplitude, 200 mT. と Magic Green のみの ESR スペクトル（黒, 溶媒：CH_2Cl_2）

S5 Computational details

Quantum mechanical calculations. Full structural model of 1 was adapted for the quantum chemical calculations to elucidate the electronic states and reaction mechanisms. The Ru complex, referred as [**1**]$^{2+}$, is composed of [Ru(OH$_2$)(bpy)(thaq)]$^{2+}$ (bpy=2,2'-bipyridine, thaq = 1-(2,2':6',2''-terpylyd-4'-yl)-8-(2,6-di-*tert*-butyl-*p*-hydroxyphenyl)anthraquinone), where the tpy and 2,6-di-*tert*-butyl-*p*-hydroxyphenyl)anthraquinone moieties are bridged by anthraquinone. Water molecules surrounding the Ru and phenol centres are included explicitly to the model. Density functional theory (DFT) in combination with the implicit continuum solvation model (COSMO) with ε = 78.4 for water solvent were employed. The DFT is treated as unrestricted open-shell with the B3LYP functional and Grimme's dispersion correction (UB3LYP-D3). Used basis sets are valence double zeta (VDZ) basis sets and valence double zeta polarized (VDZP) basis sets for full geometry optimizations and total energy evaluations, respectively. More specifically, the VDZ basis set represents LANL-2DZ for Ru and 6-31G for other atoms, and the VDZP represents LANL-2DZ for Ru and 6-31G(d) for other atoms. We have shown that the theoretical level of UB3LYP-D3/VDZP can predict reliable relative energies and physical properties for metal complexes and metalloenzymes.[7-9] NWChem 6.8 program package was used for all calculations.[10] The molecular structures shown in the figures were drawn using the VMD program.[11]

Table S3. Relative energies (kcal mol⁻¹) of the product and transition states during the O–O bond formation in various oxidizing species. The molecular structures are shown in Figure S11.

Name	Oxidizing Species	ΔE(product)	$\Delta E^{\neq}$(transition state)
a	Ru^{IV}=O, OH$^-$	18.7	21.6
b	Ru^{V}=O, OH$^-$	-4.2	23.0
c	Ru^{IV}=O, phenol cation radical, OH$^-$	-1.9	22.3
d	Ru^{IV}=O, phenoxyl radical, OH$^-$	22.7	27.6
e	Ru^{IV}=O, H$_2$O	10.2	58.2
f	Ru^{V}=O, H$_2$O	-34.0	24.7
g	Ru^{IV}=O, phenol cation radical, H$_2$O	3.6	49.3
h	Ru^{IV}=O, phenoxyl radical, H$_2$O	22.9	56.7
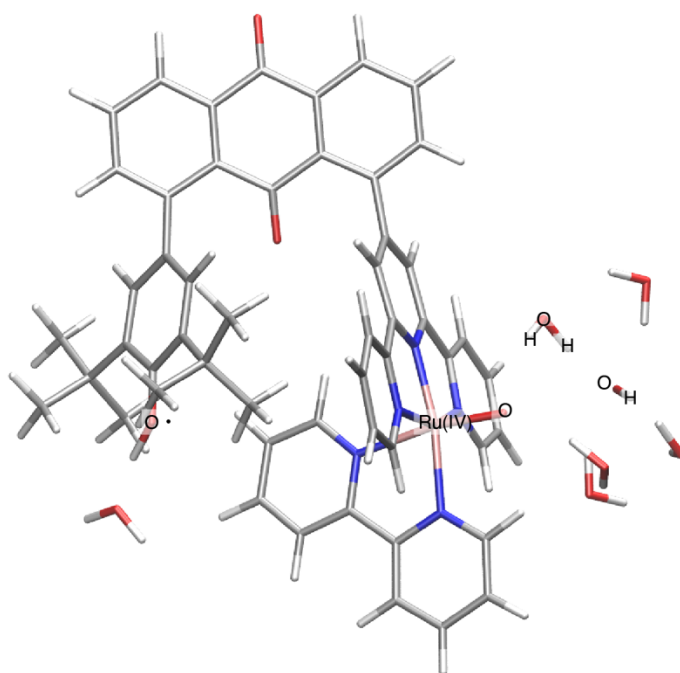
Figure S13. Molecular structure of the Ru complex [**1**]$^{2+}$ used for the theoretical calculations. Color code used: Ru, pink; O, red; N, blue; C, gray; and H, white
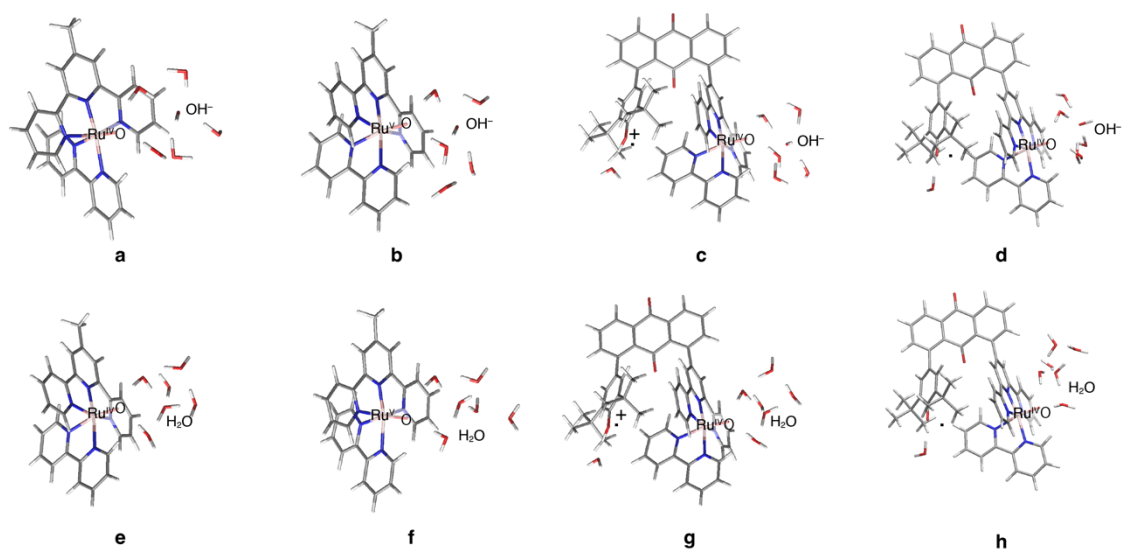
Figure S14. Optimized molecular structures of various oxidizing states in the Ru complex. Characteristics of these species are listed in Table S3
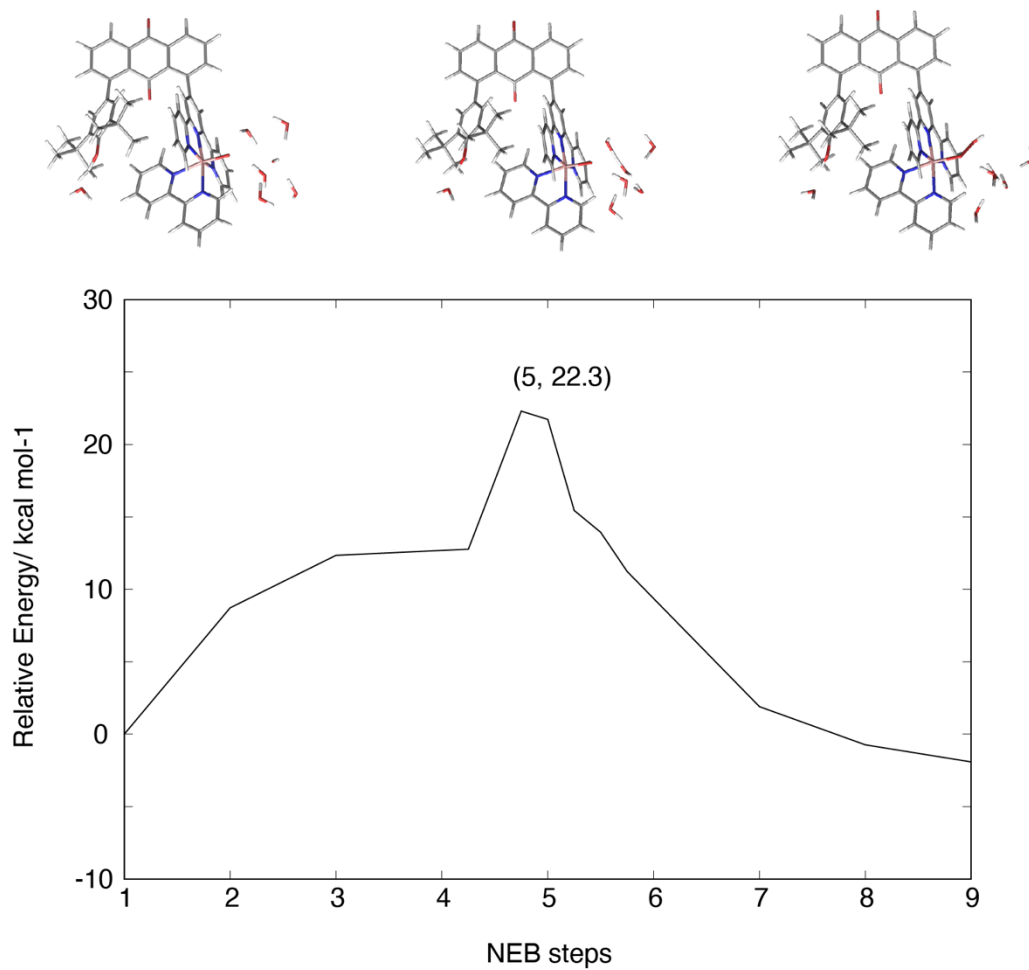
Figure S15. Energy profile of the O-O bond formation in **c**. Transition state is located at the NEB step 5 with the relative energy of $\Delta E^{\neq}$=22.3 kcal mol^{-1}. Optimized molecular structures at the reactant (NEB step 1), transition (NEB step 5) and product (NEB step 9) states are shown at the top part.
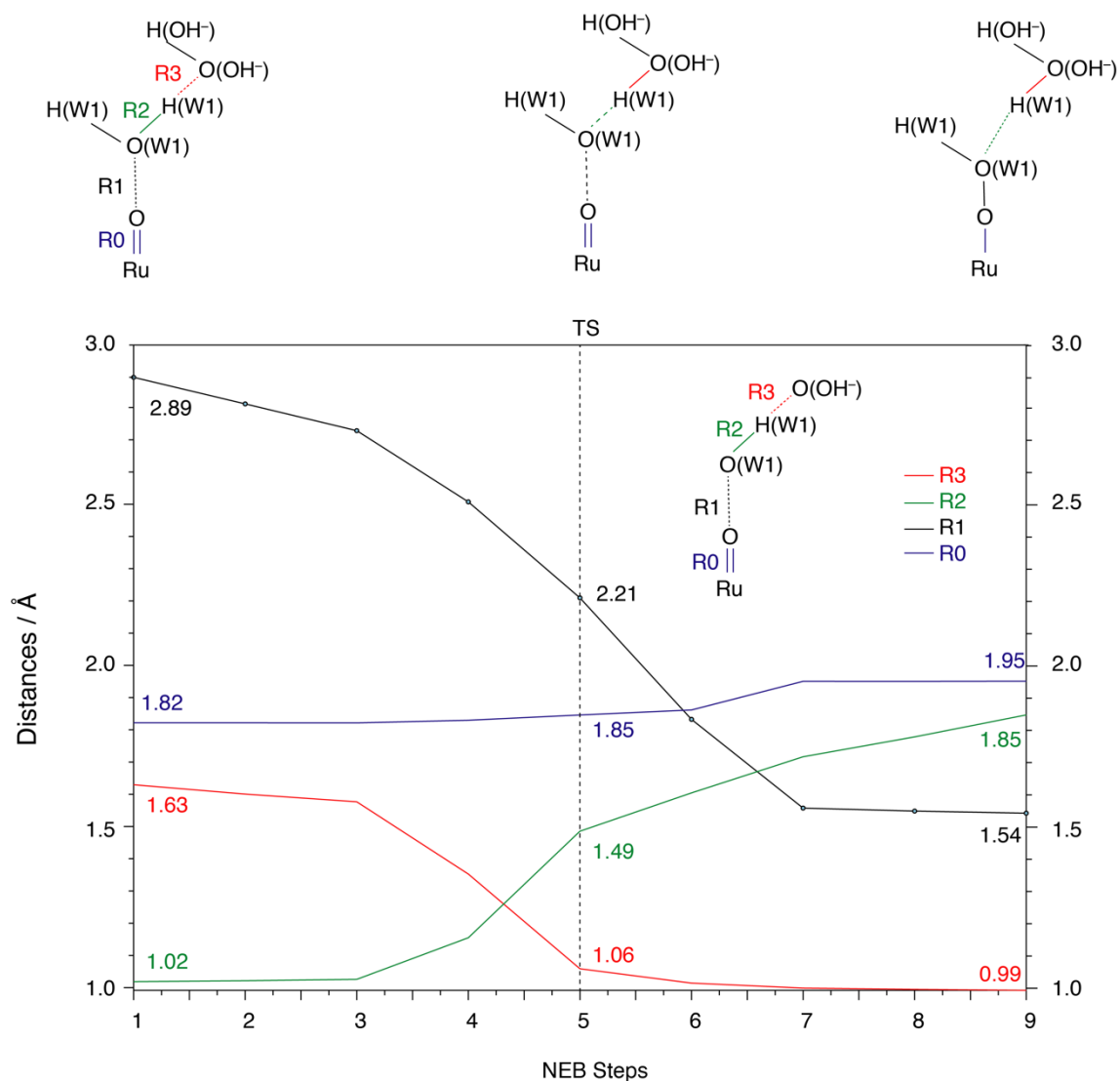
Figure S16. Changes of key atomic distances during the O-O bond formation in **c**. In the early stage before the TS at the NEB steps 1-5, OH⁻ moiety get close to the Ru-Oxo center via proton transfer (movement of H(W1)). At the TS, NEB step 5, the O atom of Ru-Oxo and O atom of OH⁻ get closer to form a covalent bond, and at the product state, NEB step 9, Ru-O-O-H species is formed.
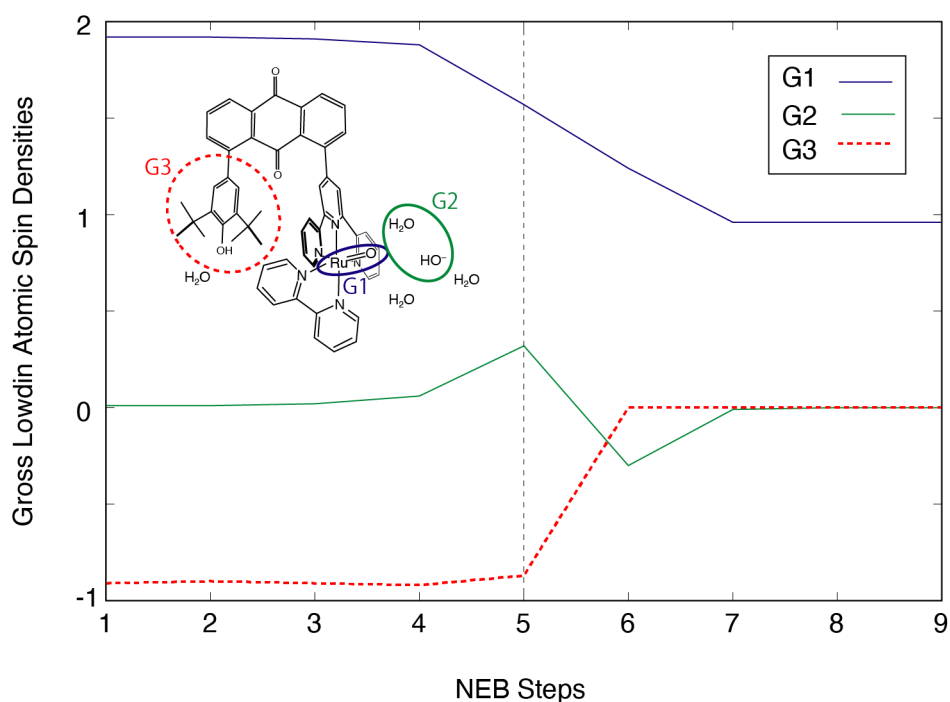
Figure S17. Löwdin atomic spin densities along the O-O bond formation in **c**. Each plot corresponds to the gross value for the moiety of (G1) Ru=O (blue color), (G2) OH⁻ and Wat1 (green color) and (G3) THAQ (dotted red color).

S6 References

1. T. Wada, S. Nishimura, T. Mochizuki, T. Ando and Y. Miyazato, *Catalysts*, 2017, **7**, 56/51-56/16.

2. K. T. Potts and D. Konwar, *J. Org. Chem.*, 2002, **56**, 4815-4816.

3. K. J. Takeuchi, M. S. Thompson, D. W. Pipes and T. J. Meyer, *Inorg. Chem.*, 1984, **23**, 1845-1851.

4. O. V. Dolomanov, L. J. Bourhis, R. J. Gildea, J. A. K. Howard and H. Puschmann, *J. Appl. Crystallogr.*, 2009, **42**, 339-341.

5. G. M. Sheldrick, *Acta Crystallogr. A*, 2015, **71**, 3-8.

6. G. M. Sheldrick, *Acta Crystallogr. C*, 2015, **71**, 3-8.

7. Y. Murata, F. Cheng, T. Kitagawa and K. Komatsu, *J. Am. Chem. Soc.*, 2004, **126**, 8874-8875.

8. M. Shoji, H. Isobe, J-R. Shen, K. Yamaguchi, *Phys. Chem. Chem. Phys.* 2016, **18**, 11330-11340.

9. M.Shoji, H. Isobe, K. Yamaguchi, *Chem. Phys. Lett.* 2019, **714**, 219-226.

10. M. Shoji, H. Isobe, Y. Shigeta, T. Nakajima, K. Yamaguchi, *J. Phys. Chem. B,* 2018, **122**, 6491-6502.

11. M. Valiev, E.J. Bylaska, N. Govind, K. Kowalski, T.P. Straatsma, H.J.J. van Dam, D. Wang, J. Nieplocha, E. Apra, T.L. Windus, W.A. de Jong, *Comput. Phys. Commun.* 2010, **181**, 1477.

12. W. Humphery, A. Dalke, K. J. Schulten, *Mol. Graphics*, 1996, **14**, 33-38.